AALBORG UNIVERSITY

DENMARK

Investigation of Drag Force on Fibres of Bonded Spherical Elements using a Coupled CFD-DEM Approach

Jensen, Anna Lyhne; Sørensen, Henrik; Rosendahl, Lasse Aistrup; Adamsen, Per; Lykholt-Ustrup, Flemming

[Link to publication from Aalborg University](#)

Investigation of Drag Force on Fibres of Bonded Spherical Elements using a Coupled CFD-DEM Approach

Anna Lyhne Jensen[1], Henrik Sørensen[1], Lasse Rosendahl[1], Per Adamsen[2], Flemming Lykholt-Ustrup[2] *

[1]*Aalborg University*
Pontoppidanstræde 111, 9220 Aalborg Øst
alj@et.aau.dk

[2]*Grundfos*
Poul Due Jensens Vej 7, 8850 Bjerringbro

Abstract

Clogging in wastewater pumps is often caused by flexible, stringy objects. Therefore, simulation of clogging effects in wastewater pumps entails simulation of such flexible objects and the interaction between these objects and fluid in the pump. Using a coupled CFD-DEM approach, the flexible object can be modelled as a multi-rigid-body system using bonded spherical DEM particles. However, the flexible objects are not resolved by the CFD mesh, and therefore modelling of fluid forces on the flexible object becomes a key issue. This study investigates the modelling of fluid forces on a rigid fiber as the first step towards simulation of clogging effects using CFD-DEM. The drag force on cylinders of finite aspect ratios $2\leq \beta \leq 40$ for Reynolds numbers in the range $0.1 \leq \text{Re} \leq 1000$ at an angle normal to the flow direction are investigated. The drag is examined along the span of the cylinders and end effects are quantified. The drag coefficient on the resolved cylinder is compared to a CFD-DEM simulation of a flexible fiber made by a chain of bonded spherical discrete elements, using a free steam drag formulation on each particle. Based on the results, a drag force model can distinguish between the outermost segments and the segments in the center of the fiber.

Keywords: CFD-DEM, clogging, flexible fiber, circular cylinder, drag

1.   Introduction

Clogging in wastewater pumps causes reduced flow, increased power consumption, and ultimately a complete stop of the pump. In the wastewater pumping stations of Berlin, around 12000 failure events occurs every year, the majority of these failures caused by clogging of the pumps [1]. The cost of system maintenance and downtime, underlines the importance of minimizing the occurrence of these failures. Clogging is commonly caused by flexible objects in wastewater such as plastic bags, sanitary items, and different types of textile and cleaning cloths. Wastewater pumps are designed to be resistant to clogging, however the design is usually based on experience and expensive experiments on prototypes using artificial wastewater. By simulating clogging effects the design process will be significantly facilitated and clogging effects can be studied in detail. Consequently, the long term aim of this work is an industrial tool applicable for simulation of clogging effects. In experimental investigations of clogging effects, dusters are commonly used to create the artificial wastewater [1, 2]. The long term aim is to replicate these experiments, and as the first step a flexible fiber is investigated.

The Discrete Element Method (DEM) was developed for simulation of granular media [3]. However, at present day commertial DEM software has been developed with options of both bonded particles and coupling to CFD software readily available. This represents an interesting option of fiber modelling as multi-rigid-body systems with fluid-fiber interaction to simulate fiber suspensions in complex fluid flow. The CFD-DEM approach using ANSYS Fluent and EDEM from DEM Solutions resembles previous fiber suspension models, but within a framework already designed for parallel, high efficiency computing. Keeping in mind the final aim of developing an industrial tool, software already used in the pump industry is a clear advantage. How-

ever, this requires implementation of well validated fluid-fiber interaction force models.

In the paper and pulp industry, extensive work has been done in order to simulate fluid flow with flexible pulp fiber suspensions using multi-rigid-body systems, where the fiber is divided in to rigid segments of spherical, cylindrical or elliptical shape. These rigid segments are bonded and form flexible fibers. Therefore the work focuses, among other things, on the fundamental issue of determining how to model the fluid forces on the individual fiber segments. Yamamoto and Matsuoka (1995) [4] modelled suspended fibers as chains of spherical particles and included a model of fiber mechanics and a model of the influence of the fluid on the fiber. In their early work they used a free draining approximation and the hydrodynamic force on each sphere was assumed proportional to the relative velocity. Later, Lindström and Uesaka (2007) [5] modelled a flexible fiber as a chain of cylindrical segments and investigated fiber-fluid interactions in the non-creeping flow regime by simulating cross flow around a circular cylinder with an aspect ratio of 40. End effects were not included as the domain did not exceed the cylinder ends. A similar approach is used in the present work, where cylinders of different aspect ratios will be simulated at various Reynolds numbers to determine the drag coefficient. This type of simulation, with a background in paper and pulp industry and fiber supensions, has also been made by Vakil and Green [6], who investigated the flow around cylinders of different aspect ratios and orientations, including end effects. Reynolds numbers between $1 \leq \text{Re} \leq 40$ were simulated at different angles. Also Rajani et al. (2009) [7] investigated the laminar flow around circular cylinders. Additionally, fluid forces on simple shapes such as spheres and cylinders have been investigated experimentally by Weiselsberger (1922) [8] and Jayaweera and Mason (1965) [9] among others.

Using DEM, the fiber will be modelled as a chain of rigid spherical segments as sketched in Fig. 1. A good approximation

of fiber shape would be the cylindrical shape also sketched in Fig. 1. In order to determine a model for the fluid force on each segment the fluid forces on cylinders of different aspect ratios are investigated using CFD. In the paper and pulp industry the relative flow is in the non-creeping regime with Re_P in the order of 1-100 [10]. This is with pulp fiber diameters in the range 20-40 μm and length of 300-3000 μm. Pulp fines are typically 20-40 μm with a diameter of 40-300 μm. Objects in wastewater, such as dusters, have densities close to the density of water. Therefore, the relative velocity between the objects and the fluid is expected to be low, leading to low Reynolds numbers in a similar range as those described for paper and pulp industry.
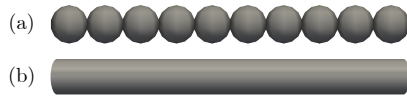

Figure 1: (a) DEM fiber formed by a chain of spherical DEM particles interconnected by bonds. (b) Fiber approximated by a cylindrical shape, which is investigated using CFD. The cylinder is divided into n segments to investigate the force distribution over the span of the cylinder.

Cylinders with aspect ratios of $\beta = [1, 2, 5, 10, 40]$ at Re = [0.1, 1, 10, 40, 100, 1000] and orientation normal to the flow direction are simulated. Fluid-fiber interaction forces and the importance of aspect ratio and end effects are estimated. Using the CFD-DEM approach, the fiber is not resolved by the CFD mesh and the modelling of the fluid force is therefore crucial for the accuracy of the coupled simulation. Using spherical particles in the DEM model of the fiber, the number of particles constituting the fiber corresponds to the aspect ratio of the fiber. Since the fiber is flexible, a variation of fluid forces across the span of the fiber will lead to fiber deformation. As the fiber deforms, drag must be modeled on the new shape. This is done by dividing the fiber into segments and using the angle between each segment and the relative fluid flow to determine the drag coefficient. Therefore, simulation of cylinders in different angles is necessary for a complete model. However, the present work covers cylinders in normal to the flow.

Firstly, the CFD simulations of cylinders of different aspect ratios are described. Secondly, the CFD simulations are validated by experimental results from different authors and the results are presented and the CFD-DEM modelling of a submersed fiber is described. Finally, perspectives for future work are discussed.

2.   CFD Simulation of Cylinders

CFD simulations of cylinders of aspect ratios in the range $\beta = [1, 2, 5, 10, 40]$ and Re = [0.1, 1, 10, 40, 100, 1000] are conducted to determine the drag force along the span of the cylinder and to investigate the importance of end effects to determine if these effects should be included in the drag model used in the CFD-DEM coupling. Furthermore the results of the 3D simulations are compared to results of 2D simulations corresponding to $\beta \rightarrow \infty$. Vortex shedding starts at Re $\approx$ 50. Therefore, simulations with Re < 50 where run as steady simulations.

2.1.   CFD Mesh

The computational domain is presented in Fig. 2. The grey plane marked in the figure corresponds to the domain used for 2D simulations. The size of the computational domain is based on the domain described by Vakil and Green (2009) [6], however the width of the domain in the z-direction is doubled to ensure domain size independence for low Reynolds numbers. A mesh

independence study for the 2D case was carried out for Re = 10, Re = 100, and Re = 1000, and showed a deviation of less than 2 % to the results using a refined mesh. A section of the CFD mesh close to the cylinder is presented in Fig. 3.
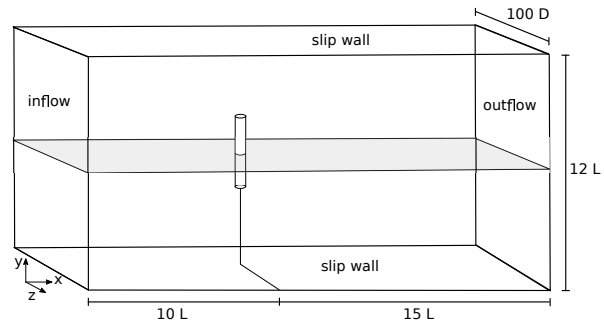

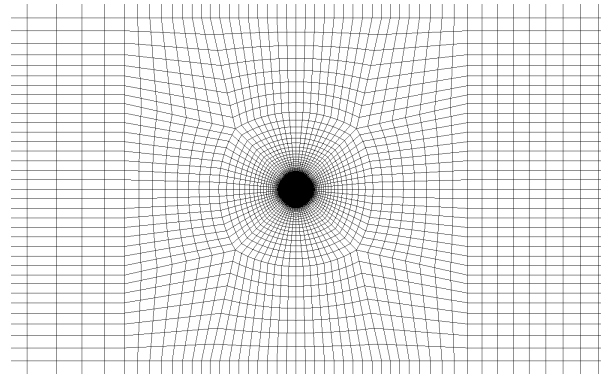Figure 2: Computational domain based on [6]. The fluid moves in the positive x-direction.

Figure 3: Section of the CFD mesh close to the cylinder.

3.   Validation

In order to validate the 2D simulations, the result of drag coefficient as function of Reynolds number is compared to numerical results by Rajani et al. (2009) [7] and experimental results by Weiselsberger (1922) [8] and Jayaweera and Mason (1965) [9]. The comparison is presented in Tab. 1 and Fig. 4. The results show good agreement between present simulation and experimental results of other authors with the largest deviation being -32 % at Re = 0.1 to the numerical results by Ref. [7]. However, the deviation to the experimental results at Re = 0.1 is lower, with a deviation of 4 % to Ref. [8] and a deviation of -9 % to [9]. Note that the experiment by Ref. [9], was conducted at Re = 0.08 and therefore the result is expected to slightly overestimate the drag coefficient at Re = 0.1, which might cause the deviation. At Reynolds numbers 1-100 the largest deviation is -12 % to the experiments by Ref. [8] at Re = 100. However, the result lies between the experimental result by Ref. [8] and the numerical result by Ref. [7] and is therefore considered reasonable. At Re = 1000 the CFD results overestimates the drag coefficient with 23 % and 28 % respectively compared to the experimental results. The deviation at Re = 1000 is in good agreement with references stating that the importance of 3D effects increases with Reynolds numbers, and that the pressure force is usually over-predicted at higher Reynolds numbers [7]. This is also evident
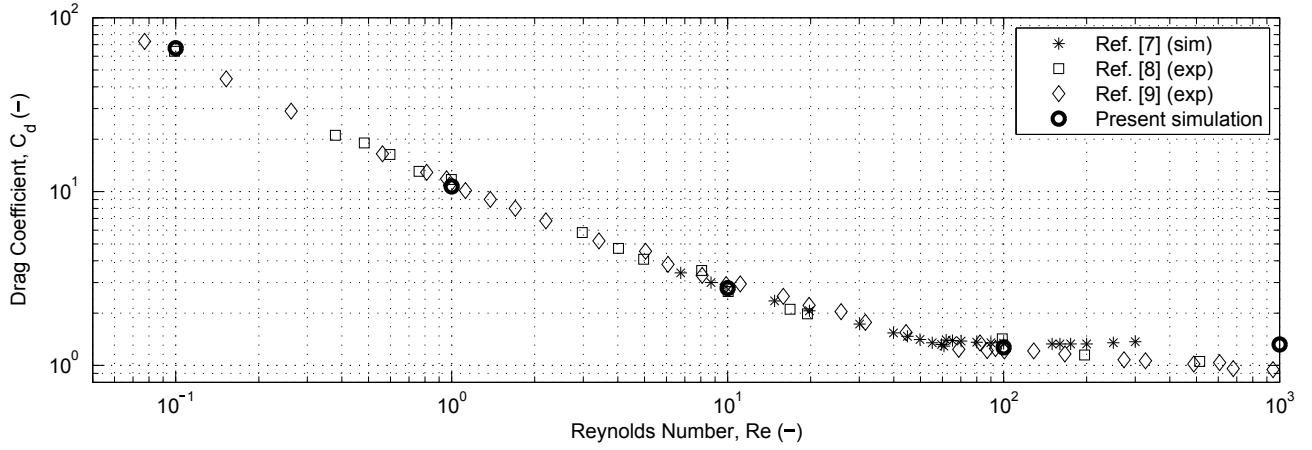
Figure 4: Comparison of present 2D simulation with numerical results by Ref. [7] and experimental results by Ref. [8, 9].

Table 1: Comparison of present 2D simulation with 3D simulation of a cylinder with $\beta = 40$, numerical results by Ref. [7] and experimental results by Ref. [8, 9], including calculated deviations.

Re	2D	$\beta = 40$	diff. (%)	Ref. [7]	diff. (%)	Ref. [8]	diff. (%)	Ref. [9]	diff. (%)
0.1	66.7	66.8	-0.1	87.8	-32	64.1	4	73.0 (Re = 0.08)	-9
1	10.7	10.7	0	11.4	-7	11.7	-9	10.8	-1
10	2.78	2.75	1	2.84	-2	2.66	4	2.92	-5
40	1.51	1.49	1	1.54	-2	-	-	1.55	-3
100	1.27	1.17	8	1.34	-6	1.42	-12	1.21	5
1000	1.32	1.01	23	-	-	1.01	23	0.946	28

from the agreement between the results of the 3D simulation of a cylinder with $\beta = 40$, which is consistent with the experimental results by Ref. [8, 9]. The consistency between 2D results and 3D results for a cylinder with $\beta = 40$ is very good until Re = 100, with deviations of less than 1 % in the drag coefficient.

The numerical results of drag coefficient as function of Reynolds number for cylinders of different aspect ratio are presented in Fig. 6, which also includes numerical results by Vakil and Green (2009) [6] for seven Reynolds numbers and four different aspect ratios. A more detailed overview of the results of the present work is given in Tab. 2. The present simulations underestimate the drag coefficient slightly compared to the numerical results by presented in Ref. [6]. The deviation is independent of the Reynolds number, and is between 4 and 9 %.

The impact of the cylinder aspect ratio on the drag coefficient is further illustrated in Fig. 5. The drag coefficient increases as the aspect ratio decreases for Reynolds number of 10 and below. Consequently, the lower the Reynolds number, the larger the aspect ratio needs to be to reach the a drag coefficient similar to the 2D result. At Reynolds numbers around 40 the 2D result deviates only 5 % from the 3D result with an aspect ratio of 2. For Re = 100 and Re = 1000 the drag coefficient slightly increases with the aspect ratio.

The 3D results for Re = 1000 are significantly lower than the 2D results, which are overestimating the pressure force. However the 3D results for $\beta = 40$ are close to the experimental results. The overestimation in the 2D results is evident from Fig. 5, where the 3D results are significantly below the 2D result for all aspect ratios.

Based on the comparison between presented simulations and experimental and numerical result, the simulations are considered valid, and the spanwise distribution of forces can be investigated.
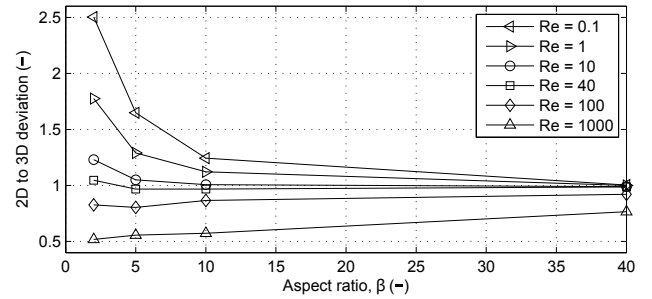

Figure 5: Impact of cylinder aspect ratio on the drag coefficient at Reynolds numbers in the range 0.1 to 1000.

4. Spanwise Force Distribution

Different drag models for CFD-DEM simulations have been developed, however these are developed for spherical or close to spherical particles and do not take particle bonds into account. Therefore, application of these to the simulation of flexible fibers is not appropriate. One of the simplest existing drag models is the free stream drag model, which uses a classical formulation of the drag coefficient as function of Reynolds number for a sphere, as given in Eq. (1).

$$c_{\mathrm{d}} = \begin{cases} 24/Re, & \text{if } Re \leq 0.5; \\ 24 \cdot \left(1 + 0.15 \cdot Re^{0.687}\right)/Re, & \text{if } 0.5 < Re \leq 1000; \\ 0.44, & \text{otherwise.} \end{cases}$$
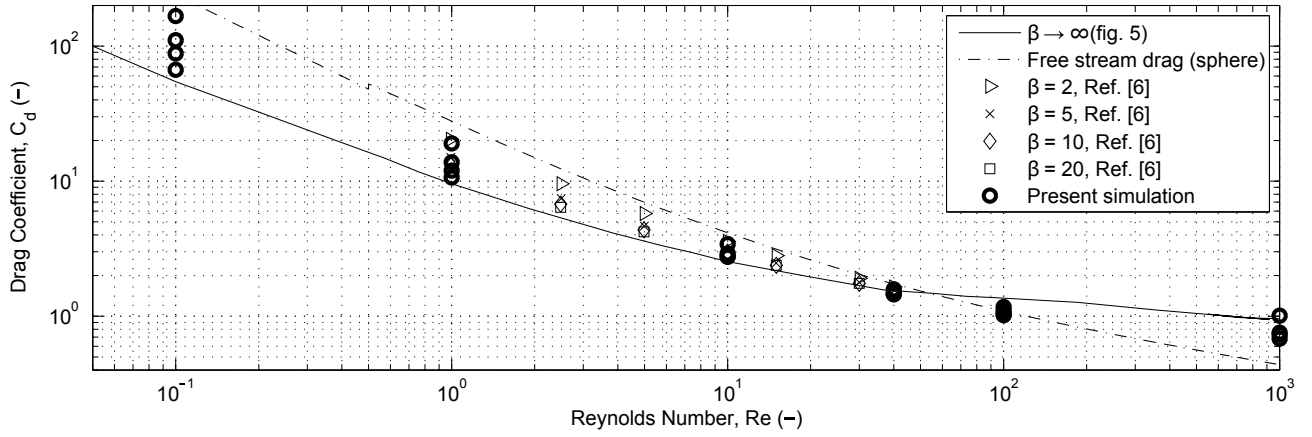
$$(1)$$

Figure 6: Drag coefficient as function of Reynolds number for cylinders of different aspect ratio.

Table 2: Drag coefficient of cylinders with aspect ratios at different Reynolds numbers, and comparison to results from Ref. [6].

| Re	2D	$\beta = 2$	Ref. [6]	$\beta = 5$	Ref. [6]	$\beta = 10$	Ref. [6]	$\beta = 40$
0.1	66.7	167	-	110	-	88.2	-	66.8
1	10.7	19.0	20.4	13.8	15.0	12.0	13.0	10.7
10	2.78	3.42	3.58	2.92	3.07	2.80	2.99	2.75
40	1.51	1.58	1.65	1.46	1.57	1.46	1.56	1.49
100	1.27	1.05	-	1.02	-	1.10	-	1.17
1000	1.32	0.683	-	0.734	-	0.756	-	1.01

where Re is based on the relative velocity between fluid and particle and the diameter of the particle. The free stream drag model is illustrated with the dashed line in Fig. 6. It is seen in the figure that the drag coefficient of a sphere is higher than the drag coefficient for cylinders of aspect ratios down to 2 until Re ≈ 50, where it intersects with the drag coefficient of cylinders. Modelling the fluid force on the fiber using the existing formulation will lead to an overestimation, and a constant fluid force throughout the span of the fiber for Re < 50, and an overestimation for Re > 50. A new model can be created by varying the drag coefficient depending on the position of each segment, therefore the spanwise distribution of the drag coefficient for the individual segments is of interest.

Figure 7-11 show the drag coefficient as function of spanwise location x/L to investigate the influence of choosing a constant drag coefficient independent of the spanwise location. The drag coefficient for each segment is determined as given in Eq. 2.

$$C_{\mathrm{d,i}} = \frac{2 \cdot F_{\mathrm{x,i}}}{\rho \cdot u^2 \cdot A_{\mathrm{i}}} , \qquad (2)$$

where $F_{\mathrm{x,i}}$ is the total force in the x-direction on segment i, ρ is the fluid density, u^2 is the fluid inlet velocity and A_{i} is the area of segment i of the cylinder for which the drag coefficient is calculated.

Figure 7 shows the spanwise distribution of the drag coefficient for Re = 0.1. The figure illustrates how the drag coefficient is largest at the ends of the cylinder and reaches a value close to constant in the remaining part at the middle of the cylinder. The tendency is similar for all the included aspect ratios. This distribution is similar to the distribution at Re = 1 and Re = 10 in Fig. 8 and 9 respectively, where the drag coefficient is also highest at the outermost segments of the cylinder. However, the shift in overall drag coefficient depending on the aspect ratio is largest for Re = 0.1, which can also be seen by comparing Fig. 7-9.
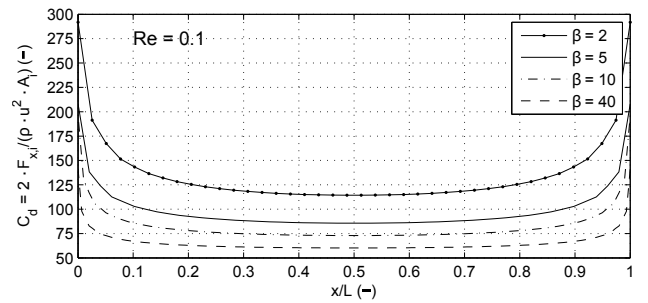
Figure 7: Drag coefficient as function of spanwise location on the cylinder at Re = 0.1.
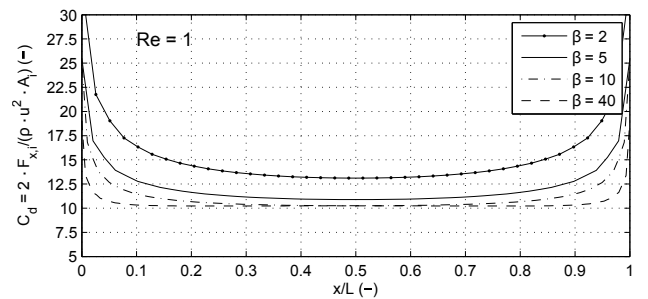
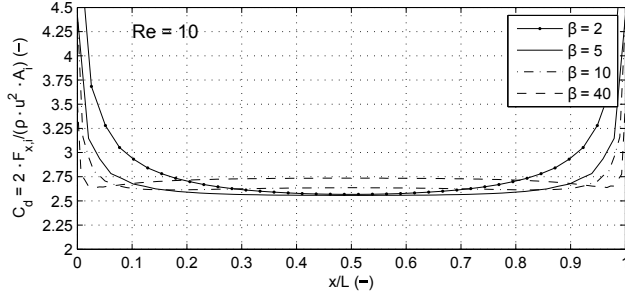Figure 8: Drag coefficient as function of spanwise location on the cylinder at Re = 1.

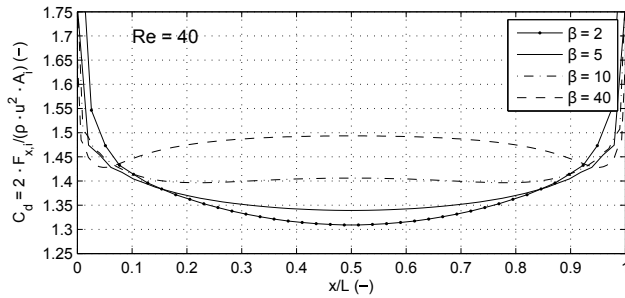Figure 9: Drag coefficient as function of spanwise location on the cylinder at Re = 10.

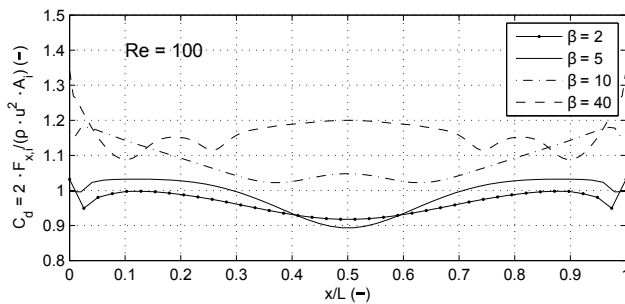Figure 10: Drag coefficient as function of spanwise location on the cylinder at Re = 40.

Figure 11: Drag coefficient as function of spanwise location on the cylinder at Re = 100.

As the Reynolds number is increased to 40, the distribution of the drag coefficient along the span changes significantly with the aspect ratio of the cylinder as illustrated in Fig. 10. At low aspect ratios the drag coefficient reaches a minimum in the center, but as the Reynolds number increases to 40 the drag coefficient at the center of the cylinder reaches a local maximum. The coefficient is still largest at the outermost segments of the cylinder. At a Reynolds number of 100 transient phenomena occurs and the drag coefficient distribution changes significantly. This can be seen in Fig. 11.

The plotted values in Fig. 11 are average values due to the transient behavior of the flow. It is seen that the drag coefficient varies along the span, however the variation is less significant than the variation along the span for lower Reynolds numbers.

5.   Simulation of Fiber Suspensions using CFD-DEM

The CFD-DEM simulation of fluid-fiber interaction consists of 3 main parts: DEM modelling of the fiber, CFD modelling, and CFD-DEM coupling. The present work focuses on the coupling, which has a major importance due to a low density ratio between fiber and fluid, which makes the conservative forces less influential.

The spherical particles in the modelled fiber are connected by bonds with a defined normal and shear stiffness and break criteria. In this case, for comparison to a resolved cylinder, the fiber is modelled as rigid.

5.1.   CFD-DEM Fluid-Fiber Coupling

The coupling between EDEM and ANSYS Fluent uses Fluents existing Eulerian multiphase model, but includes additional sets of continuity and the volume fraction. The momentum exchange between the fluid and the particle phase is determined based on models of fluid forces. In the present work only drag is included.

Figure 12 illustrates a fiber of 10 particles in a CFD grid. To investigate the drag force along the span of this fiber using the existing free stream drag model given in Eq. (1), coupled simulations of the fiber falling in fluid were conducted.
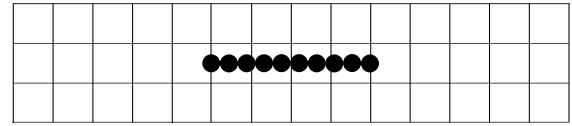
Figure 12: Sketch of a fiber of bonded DEM particles in a CFD mesh.

The results of these simulations at the Reynolds numbers investigated for the cylinder using CFD are presented in Fig. 13. It is seen that the drag coefficient is constant over the span of the fiber of spherical particles and follows the free stream drag model as expected.
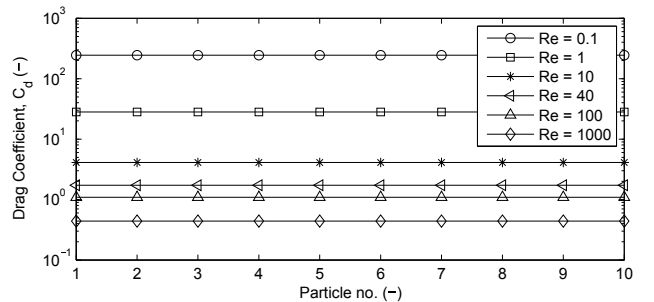
Figure 13: Drag coefficient on fiber of 10 bonded DEM particles in a coupled simulation.

6.   Perspectives

A description of the spanwise distribution of fluid forces for a cylinder normal to the flow is not adequate for the modelling of fluid forces on a fiber, since the angle between the fiber and the relative fluid velocity is continuously changing and the drag force is dependent of the orientation for non-spherical particles. Therefore, a more detailed description including different angles

is required before implementation. Drag on non-spherical particles is a common problem studied by several authors and several formulations of the drag as function of angle of attack has been suggested. Each particle will be seen as a cylinder segment, and the angle between the bonds from the particle to the neighbouring particles will determine the angle of attack.

Using the CFD, an inherent compromise between the CFD cell size and the size of the unresolved DEM particles is made. The size of the DEM particles should be smaller than the size of the CFD cell. However, simulation of flow in complex geometries such as a pump requires small cells in parts of the geometry. Furthermore, very small particles compared to cell size does not allow for diferentiation between the drag on the individual particles.

The long term aim is to move from modelling of fluid forces on flexible fibers to modelling of fluid forces on surfaces such as a duster to use the force models to simulate clogging effects in wastewater pumps.

7.   Conclusion

Simulation of circular cylinders in 2D and 3D with different aspect ratios shows good correspondence in terms of drag coefficient with experimental and numerical results presented by [8, 9, 7]. The maximum deviation of 32 for Re = 0.1 and a general deviation in the order of 1-7 %, noting that the results of these authors had similar deviations.

Investigation of the spanwise drag coefficient at different Reynolds numbers and aspect ratios shows that the drag coefficient increases significantly as the aspect ratio decreases for low Reynolds numbers. On the other hand the drag coefficient is almost independent of aspect ratio for Re = 40 and the drag coefficient decreases slightly with the aspect ratio for Reynolds numbers of 100 and 1000.

For low Reynolds numbers, the outermost segments of the cylinder experiences the highest drag coefficient. The variation is nearly independent of aspect ratio at these Reynolds numbers. At a Reynolds number of 40, a difference in aspect ratio changes the spanwise drag coefficient distribution, and a local peak of C_d occurs in the central segments of the fiber for aspect ratios of 10 and 40.

Further investigation on different angles and Reynolds numbers is necessary before a drag force model, which can distinguish between the outermost segments and the segments in the center of the fiber, can be developed.

References

[1] Pöhler, M., Gerlach, S., Höchel,, K., Mengdehl, T., Thamsen, P.U., Linking efficiency to functional performance by a pump test standard for wastewater pumps, *Proceedings of the ASME-JSME-KSME Joint Fluids Engineering Conference 2015*, pp. 2529-2535, 2015.

[2] Thamsen, P.U., Cutting clogging in wastewater, *World Pumps*, 2009, 511, pp. 22-25, 2009.

[3] Cundall, P., Strack, O. A discrete numerical model for granular assemblies, *Geotechnique*, 29, pp. 47-65, 1979.

[4] Yamamoto, S., Matsouka, T., Dynamic simulation of fiber suspensions in shear flow, *J. Chem. Phys*, 102, pp. 2254-2260, 1995.

[5] Lindström, S.B., Uesaka, T., Simulation of the motion of flexible fibers in viscous fluid flow, *Physics of Fluids*, 19, pp. 113307, 2007.

[6] Vakil, A., Green, S.I. Drag and lift coefficients of inclined finite circular cylinders at moderate Reynolds numbers, *Computers & Fluids*, 38, pp. 1771-1781, 2009.

[7] Rajani, B.N., Kandasamy, A., Majumdar, S. Numerical simulation of laminar flow past a circular cylinder, *Applied Mathematical Modelling*, 33, pp. 1228-1247, 2009.

[8] Weiselsberger, C., *New data on the laws of fluid resistance*, 84, Technical Notes, National Advisory Committee for Aeronautics, 1922.

[9] Jayaweera, K.O.L.F., Mason, B.J., The behaviour of freely falling cylinders and cones in a viscous fluid, *Journal of Fluid Mechanics*, 22, pp. 709-720, 1965.

[10] Lindström, S.B., *Modelling and simulation of paper structure development*, PhD thesis, Mid Sweden University, Sundsvall, Sweden, 2008.